AMS Home   Journals Home   Journal Archive   Subscribe   For Authors   Help   Advanced Search | Search | Go |

Full Text View

Spectrum of Wind-Driven Baroclinic Fluctuations of the Ocean in the Midlatitudes

J. Sirven, C. Frankignoul, G. de Coëtlogon, and V. Taillandier

Laboratoire d'Océanographie Dynamique et de Climatologie, CNRS/ORSTOM/Université Pierre et Marie Curie, Paris, France

ABSTRACT

In the midlatitudes, the thermocline depth variations are largely due to Rossby waves of first baroclinic mode forced by stochastic wind stress. The frequency spectrum of this oceanic response is investigated with a simple model, with emphasis on the impact of (i) the horizontal mixing, (ii) the zonal variations of the forcing, and (iii) the nonlinearity due to variations of the Rossby wave celerity in function of the thermocline depth. Horizontal mixing, which acts here as a frequency-dependent Newtonian damping, smoothes the singularities of the spectrum computed in a linear nondissipative case and slightly increases the slope of the spectrum at periods shorter than 10 yr. Considering a wind stress with a continuous spectrum also smoothes the response spectrum and modifies the power at decadal and interdecadal frequency: it alters its dependence on the distance from the eastern boundary. A spectral peak appears when the forcing has a dominant zonal scale, but this peak disappears in more realistic cases. The nonlinearity included in Rossby wave celerity induces energy transfers from decadal frequency to annual frequency, thereby whitening the frequency spectrum at periods ranging from 0.5 to 5 yr. These features lead to a better agreement with GCM simulations and observations.

1. Introduction

In the midlatitudes, the variability of the ocean thermocline is dominated by decadal timescales. Levitus (1989) found large decadal changes in hydrographic observations of the upper 1000 m of the North Atlantic Ocean, and Joyce and Robbins (1996) found in-phase decadal variability in temperature and salinity in the thermocline near Bermuda. There is increasing evidence that much of this large-scale variability in the thermocline is wind driven and could reflect the natural variability of the atmosphere via stochastic wind stress forcing, as suggested by Frankignoul et al. (1997, hereafter FMZ). In their simple model (a linear inviscid model with a flat bottom, a mean state at rest, and zonally independent forcing) the baroclinic response of the ocean to wind forcing consists of the superposition of a forced solution and long Rossby waves that propagate westward. The predicted spectrum decays as ω^{-2} at annual timescales and flattens at decadal timescales, with a succession of peaks and troughs that correspond to in-phase and out-of-phase relations between the forced and the free response. Its envelope is in good agreement with the spectrum computed

in an extended integration of the ECHAM1/LSG coupled GCM in the North Atlantic subtropical gyre, with a rather similar dependence on longitude and latitude. However, the consistency of these baroclinic predictions with the observed spectrum of sea level changes and temperature fluctuations near Bermuda is less convincing, as illustrated in Fig. 1 ◐⬛, since the observed spectrum decays like ω^{-1} or $\omega^{-1.5}$ at high frequency. The effect of zonally varying forcing has been discussed by Jin (1997), who considered the influence of a large-scale standing wind stress pattern and showed that it created a spectral peak in the oceanic response.

Here, we investigate how a more realistic setting will modify the frequency spectrum of the wind-driven response at interannual to interdecadal timescales. First, we analyze the role of dissipation, using the formulation of Qiu et al. (1997), who suggested that dissipation may be important at high latitudes by dissipating the free Rossby waves generated at the eastern boundary. Then, we consider a spectral representation of the zonal dependance of the forcing field, using a representation in terms of propagating patterns. Finally, as the Rossby wave velocity depends on the variations of the thermocline depth and thus introduces nonlinear effects, we explore the role of these effects in a simple case. We show that they induce energy transfers in wavenumber and frequency space and modify the pattern of the spectrum.

The paper is organized as follows: In section 2, we describe the model and stress its differences with that of FMZ. We consider dissipation and scale dependence of the forcing in section 3, and the impact of nonlinearity in section 4. Discussion and conclusions are given in section 5.

2. The model

We consider a time-dependent geostrophic 2.5-layer ideal-fluid model of the ventilated thermocline similar to that described in Sirven and Frankignoul (2000). A downward Ekman pumping w_e is imposed at the surface of a subtropical gyre limited by its vanishing at $y = y_N$ and $y = y_S$. The lightest layer of density ρ_1 and thickness h_1 is located south of the latitude $y_1 (y_S < y_1 < y_N)$, where the second layer of density ρ_2 and thickness h_2 outcrops. The depth $H = h_1 + h_2$ represents the base of the thermocline. The abyss is a third layer at rest, of density ρ_3 and infinite depth, to be consistent with the rigid lid imposed at the surface. The β-plane approximation is used ($f = f_0 + \beta y$). The zonal coordinate is noted x, the meridional coordinate y. The geostrophic zonal flow vanishes at the eastern boundary ($h_1 = 0$ and $H = h_2 = H_0 = 500$ m at $x = 0$) while a no-radiation condition is used at the western boundary $x = x_w < 0$.

Sirven and Frankignoul (2000) introduced the effective depth

$$\mathcal{H} = \sqrt{\frac{\gamma_1}{\gamma_2} h_1^2 + H^2}, \qquad (1)$$

where $\gamma_1 = (\rho_2 - \rho_1)g/\rho_0$ and $\gamma_2 = (\rho_3 - \rho_2)g/\rho_0$ represents the reduced gravity associated with each layer and are both much smaller than the gravity g. They showed that the velocity of the flow, averaged over the two active layers, is proportionnal to the vector $(-\partial_y \mathcal{H}, \partial_x \mathcal{H})$ (i.e., $\mathcal{H}$ is a streamline for the averaged flow) and that $\mathcal{H}$ characterizes the overall response of the thermocline to a variation in w_e. Thus, the effective depth allows one to define correctly the first baroclinic mode in the 2.5-layer model. It satisfies the evolution equation (see appendix A)

$$\frac{\partial \mathcal{H}}{\partial t} - c_1 \frac{\partial \mathcal{H}}{\partial x} = - \lambda w_e, \qquad (2)$$

where λ is a constant ($\simeq 1$), and $c_1 = +\beta \gamma_2 \lambda \mathcal{H}/f^2$. Note that the evolution equation of the baroclinic pressure in FMZ was

$$\frac{\partial p_{bc}}{\partial t} - c_{bc} \frac{\partial p_{bc}}{\partial x} = -\frac{\rho f^2}{H_{bc}} R_{bc}^2 w_e, \qquad (3)$$

where R_{bc} is the deformation radius, $c_{bc} = +\beta R_{bc}^2$ the phase speed of long Rossby waves, and H_{bc} a baroclinic depth scale that depends on the stratification (we recall that FMZ consider a nondissipative 2-layer model and assume linearity, ideal fluid, planetary geostrophy, long-wave approximation, a flat bottom at a depth $-H$, and a basic state at rest). Equation (2) is therefore similar to (3) except that it is nonlinear (the phase speed of the Rossby wave depends on the thermocline depth) and its derivation includes the mean geostrophic currents. However, if we define $\overline{\mathcal{H}}$ as the mean value of the effective depth $\mathcal{H}$ and linearize (2) around it, relation (3) is obtained by using $R_{bc}^2 = \gamma_2 \lambda \overline{\mathcal{H}}/f^2$ and $p_{bc} = a\mathcal{H}$, where $a = \rho \gamma_2 \overline{\mathcal{H}}/H_{bc}$ is about 3–4 Pa m^{-1}.

3. Effects of the dissipation and spatial variations of the forcing

To represent the influence of horizontal mixing, we follow Qiu et al. (1997) who added to the linearized momentum equations the Laplacian term $A_h R_{bc}^2 \nabla^2$, where A_h is the coefficient of the horizontal eddy viscosity. Their reasoning and computations apply here and lead to a linearized version of (2) with dissipation in the long-wave approximation. Thus, the free waves of first barolinic mode satisfy

$$\frac{\partial \mathcal{H}'}{\partial t} - c_b \frac{\partial \mathcal{H}'}{\partial x} = A_h \frac{c_b}{\beta} \nabla^4 \mathcal{H}', \qquad (4)$$

where $\mathcal{H}'$ represents the fluctuations of the equivalent depth around its mean and c_b the mean value of the Rossby wave phase speed c_1 at a given latitude. Qiu et al. showed that (4) had approximate solutions

$$\mathcal{H}' = A \exp(x/x_e) \exp[i(\omega t + k_b x)] \quad (5)$$

where $k_b = \omega/c_b$ and $x_e \simeq [(5 c_b^4 f^4)/(16 \omega^4 A_h \beta^3)]^{1/5}$ defines an e-folding distance from the eastern boundary. This distance becomes infinite at low frequency and vanishes at high frequency, as expected from a bi-Laplacian dissipation, which mainly smoothes the small spatial scales. Its behavior depends little on the particular form of the friction that was used. For example, a Laplacian term in (4) similarly leads to an e-folding distance that behaves as $\omega^{-2/3}$ (instead of $\omega^{-4/5}$). Note that (5) is solution of the wave equation

$$\frac{\partial \mathcal{H}'}{\partial t} - c_b \frac{\partial \mathcal{H}'}{\partial x} = -\frac{c_b}{x_e} \mathcal{H}', \qquad (6)$$

which is simpler than (4) and thus used below. Horizontal mixing acts as a frequency-dependent Newtonian damping.

Qiu et al. (1997) established (5) in order to better estimate the discrepancies between the theoretical and observed Rossby wave velocities, but they did not consider the influence of damping on the spectral properties of the internal ocean response. This is investigated below, together with the effects of the spatial variations of the forcing.

a. Zonally independent forcing

To represent the wind stress forcing associated with the day to day changes in the weather, we add to (6) the forcing by the Ekman pumping fluctuations $\hat{F}(x, f, \omega) \exp(i\omega t)$. The solution consists of the free, damped wave (5) plus a forced solution. For simplicity, we first investigate the case where $\hat{F}$ does not depend on x. If the forcing is a stationary random process with a zero mean and a frequency spectrum $S_F(\omega)$ defined by

$$S_F(\omega)\delta(\omega - \omega') = \langle \hat{F}(\omega)\hat{F}^*(\omega') \rangle \quad (7)$$

where the asterisk denotes the complex conjugate, the solution is

$$\mathcal{H}' = \frac{\hat{F}(\omega)}{i\omega + \omega_d}[1 - e^{+ik_b x}e^{x/x_e}]e^{i\omega t}, \qquad (8)$$

where we have imposed $\mathcal{H}' = 0$ at the eastern boundary ($\omega_d = c_b/x_e$). The response spectrum $S(\omega, x)$ is

$$S(\omega, x) = \frac{S_F(\omega)}{\omega^2 + \omega_d^2}\left[(1 - e^{x/x_e})^2 + 4e^{x/x_e}\sin^2\left(\frac{\omega x}{2\omega_d x_e}\right)\right]. \qquad (9)$$

At period longer than a month, the forcing spectrum is approximatively white so that $S_F(\omega) = S_0$ is a constant. In Fig. 2 ⊙, the response spectrum (9) (continuous line) is compared to that of FMZ (nondissipative case, dashed line), given by

$$S(\omega, x) = 4\frac{S_F(\omega)}{\omega^2}\sin^2\left(\frac{\omega x}{2c_{bc}}\right). \qquad (10)$$

In both cases, the variance is maximum at decadal periods (about 20 years in Fig. 2 ⊙), and the spectrum flattens at lower, interdecadal frequencies toward a level $S_0 x^2/c_{b(c)}^2$ which increases *quadratically* with the distance from the eastern

coast. Indeed x_e is much larger than the basin size at these frequencies and (9) becomes

$$S(x, \omega) \simeq \frac{S_0}{\omega^2 + \omega_d^2}\left[\left(\frac{x}{x_e}\right)^2 + \left(\frac{\omega x}{\omega_d x_e}\right)^2\right]$$

$$= S_0\left(\frac{x}{c_b}\right)^2. \qquad (11)$$

At higher, interannual frequencies, dissipation changes the spectrum. Since $(1 - e^{x/x_e})^2$ is always positive, it no longer vanishes at $x = 2n\pi c_b/\omega$, where the free and forced solutions are out of phase and the peaks have a reduced amplitude. Dissipation thus induces a filling-in of the gaps in the frequency spectrum. Note also that the spectral decay at interannual frequency is somewhat faster than ω^{-2} because of the exponentials, except for $x/x_e \ll -1$ when dissipation becomes dominant, in which case $S(x, \omega) = S_0/\omega^2$.

b. Zonally dependent forcing

To better represent the wind stress forcing let us represent the Ekman pumping by a superposition of harmonic components

$$\hat{F}(k, \omega) \exp[i(\omega t + kx)], \quad (12)$$

with a frequency spectrum $S_F(k, \omega) = S_F(k, 0) = S_e(k)S_0$ that now depends on the zonal wavenumber k, but is still assumed to be white at low frequencies. It is also symmetric since there can be no privileged zonal direction (Frankignoul and Müller 1979). See also Large et al. (1991), who considered seven years of European Centre for Medium-Range Weather Forecasts (ECMWF) analyses and give a frequency–zonal wavenumber spectrum at 31°N of the wind stress curl. This spectrum is symmetric at low frequencies, shows some redness at wavelengths larger than 1000 km, and a steep fall off at shorter scales). When the forcing has the form (12), (6) has a particular solution of the form $\mathcal{H}' = \&\hat{H}\text{script;}' (k, \omega) \exp[i(\omega t + kx)]$ with $\&\hat{H}\text{script;}' = \hat{F}(k, \omega)/[i(\omega - kc_b) + \omega_d]$. Using (5) and the vanishing of $\&\hat{H}\text{script;}'$ at the eastern boundary leads to

$$\hat{\mathcal{H}}' = \frac{\hat{F}(k, \omega)}{i(\omega - kc_b) + \omega_d}[1 - e^{+i(k_b - k)x}e^{x/x_e}] \qquad (13)$$

so that the power spectrum is

$$S(k, x, \omega)$$

$$= \frac{S_e(k)S_0}{(\omega - kc_b)^2 + \omega_d^2}$$

$$\times \left[(1 - e^{x/x_e})^2 + 4e^{x/x_e}\sin^2\frac{(\omega - kc_b)x}{2c_b}\right]. \qquad (14)$$

Figure 3 ⊙▬ shows (14) for the case where $S_e(k)$ has a maximum at $k_0 = 1.6 \times 10^{-3}$ km^{-1} (the corresponding wavelength is about 4000 km) and decreases as k^{-2} for large k. A peak occurs at the resonant pulsation $\omega_r = kc_b$ of a free Rossby wave of wavenumber k. For a 4000-km wavelength corresponding to the dominant synoptic scale of atmospheric variability (Holton 1992) and $c_b = 2$ cm s^{-1}, the corresponding period is about 8 yr. The amplitude of the peak increases southward since dissipation decreases but, even if dissipation vanishes, the spectrum never has a singularity because of the limited fetch. Indeed, in the latter case, (14) reduces in the vicinity of the resonant frequency to

$$S(k, x, kc_b) \simeq \lim_{\omega \to kc_b} \frac{4S_e(k)S_0}{(\omega - kc_b)^2} \sin^2\frac{(\omega - kc_b)x}{2c_b}$$

$$\simeq S_e(k)S_0\frac{x^2}{c_b^2}. \tag{15}$$

When the spectrum in Fig. 3 O= is integrated over wavenumbers, one obtains a frequency spectrum that still has a small peak at frequency $\omega \simeq c_b k_0$ (not shown). A sharper peak is found when $S_e(k)$ is concentrated in a narrow wavenumber range between $k_0 - \delta k_0$ and $k_0 + \delta k_0$. Indeed, the integration of (14) then leads to a frequency spectrum approximatively equal to

$$S(x, \omega) \simeq \frac{2\delta k_0 S_e S_0}{(\omega - k_0 c_b)^2 + \omega_d^2}$$

$$\times \left[(1 - e^{x/x_e})^2 + 4e^{x/x_e} \sin^2\frac{(\omega - k_0 c_b)x}{2c_b}\right], \tag{16}$$

which has a peak at $\omega \simeq c_b k_0$. This corresponds to the case studied by Jin (1997), although he considered a standing forcing pattern. However, power of the observed wind stress curl spectrum is somewhat more evenly distributed in wavenumber than in the example of Fig. 3 O= (e.g., Large et al. 1991). As shown below, in more realistic cases, there is no peak in the frequency spectrum of the response.

If the wind stress curl has a continuum of zonal scales between $-k_M$ and $+k_M$, the frequency spectrum can be computed from (14):

$$S(x, \omega) = \int_{-k_M}^{+k_M} \frac{S_e(k)S_0}{(\omega - kc_b)^2 + \omega_d^2}\left[(1 - e^{x/x_e})^2 + 4e^{x/x_e} \sin^2\frac{(k - k_b)x}{2}\right] dk. \tag{17}$$

(Click the equation graphic to enlarge/reduce size)

To clarify the influence of the spatial structure of the forcing, we first consider the simplest case where $S_e(k)$ equals $1/(2k_M)$ between $-k_M$ and $+k_M$ and equals 0 outside this range. Setting $(k - k_b)\, x = u$, with $k_b = \omega/c_b$ as before, (17) becomes

$$S(x, \omega) = \int_{(-k_M-k_b)x}^{(k_M-k_b)x} \frac{S_0/2k_M}{(uc_b/x)^2 + \omega_d^2}\left[(1 - e^{x/x_e})^2 + 4e^{x/x_e} \sin^2\frac{u}{2}\right] \frac{du}{x}. \tag{18}$$

As shown in Fig. 4 O=, the frequency spectrum has no peak in this case. At very low frequency, (18) simplifies into

$$S(x, \omega) = \frac{S_0}{2k_M c_b^2} \int_{(-k_M-k_b)x}^{(k_M-k_b)x} x\frac{\sin^2(u/2)}{(u/2)^2} du \tag{19}$$

since x_e can then be considered to be infinite. For large $|x|$ (larger than 3000 km), the integral can be well approximated by 2 $\int_{-\infty}^{\infty} |x| \, [\sin^2 \upsilon/\upsilon^2] \, d\upsilon = 2\pi|x|$, and we have

$$S(x, \omega) \simeq \frac{\pi S_0 |x|}{k_M c_b^2}. \tag{20}$$

If the wind stress curl has a white wavenumber spectrum, the response spectrum is white at low frequency and its level increases *linearly* with distance from the eastern boundary (Fig. 4 O=), rather than quadratically as in the case of a zonally independent forcing.

A similar computation can be done for a wind stress curl spectrum that decays at high wavenumber as k^{-2}:

$$S_F = S_0 \frac{k_M}{\pi(k_M^2 + k^2)}. \qquad (21)$$

At interdecadal frequency, it yields (see appendix B)

$$S(x, \omega) = \frac{2S_0|x|}{k_M c_b^2}\left[1 - \frac{1}{k_M|x|}(1 - e^{-k_M|x|})\right]. \qquad (22)$$

For $k_M|x| \ll 1$ (on distances from the eastern boundary much smaller than the most energetic forcing scale), the x dependence of the response spectrum is quadratic, as in FMZ where all the energy was concentrated at $k = 0$. For $k_M|x| \geq 1$, the x dependence is linear, as for a white spatial spectrum.

To illustrate a more realistic case, we have computed the wind stress curl spectrum in a simulation with a low-resolution coupled model, the ECHAM1/LSG model of the Max Planck Institute in Hambourg (e.g., von Storch et al. 1997; Zorita and Frankignoul 1997), using annual means from the last 40 years of the run at 27°N. The power is mainly concentrated in large scales, decaying as k^{-1} for wavelengths longer than 14 000 km and as k^{-2} for those that are shorter (Fig. 5a ○). As shown in Fig. 5b ○, the x dependence of the oceanic response spectrum for periods longer than 10 yr is intermediate between linear (cf. with Fig. 4 ○ and note the narrower space between the three curves for $T > 20$ yr) and quadratic (FMZ). The slope of the spectrum at high frequency is less steep than in Fig. 4 ○ and thus in better agreement with the observations. The response spectrum in the absence of dissipation shown in Fig. 5c ○ is very similar. This stresses that for a continuum of zonal scales in the forcing field, there is no gap in the frequency spectrum, even in the absence of dissipation. The x dependence of the spectra does not depend on the dissipation at very low frequency, but only on the spatial spectrum of the forcing and the latitude via the propagation velocity c_b. On the other hand, the power at near-decadal periods is reduced by dissipation.

We also computed the oceanic response spectrum of the coupled ECHAM1/LSG model at 30°N, at periods of 12.5, 20, 50, and 100 yr. The power dependence on longitudes is compared in Fig. 6 ○ with a parabola [Eq. (11)] and a straight line [Eq. (20)]. The straight line is parallel to the linear best fit (in the least squares sense) of the data. We chose $2\pi/k_M = 4000$ km, corresponding to typical wavelengths of synoptic patterns in the atmosphere. For both curves, S_0/c_b^2 is the same. This figure illustrates that taking into account the spatial dependence of the forcing in (14) leads to a better agreement with the coupled model data at decadal periods and that at lower frequency the longitude dependence is intermediate between linear and quadratic, becoming closer to quadratic at longest periods.

In the more realistic case of Fig. 5 ○, dissipation has very little effect on the oceanic response spectrum, as shown by the similarity between Figs. 5b and 5c ○. For simplicity, we thus neglect it below.

4. Impact of the nonlinearities

If, for simplicity, dissipation and the spatial variations of the forcing are neglected, (2) corresponds to a nonlinear version of FMZ. A stationary solution for a stationary forcing w_0 is

$$h_0^2 = H_0^2 + \int_0^x \frac{2f^2}{\beta\gamma_2}w_0(u)\,du = H_0^2 + \frac{2f^2 x}{\beta\gamma_2}w_0. \qquad (23)$$

The thermocline deepens westward when w_0 is negative (subtropical gyre) and shoals when it is positive (subpolar gyre). Consequently, the Rossby wave velocity increases westward in the subtropical gyre and decreases in the subpolar gyre.

In order to study the properties of this model we use below two complementary approaches. The first one consists of asymptotic expansions and is only valid if the perturbations are small. The second uses the characteristics method and is more general but requires some numerical integrations.

a. Study with asymptotic expansions

We consider a forcing $w_e(t) = w_0 + \epsilon w_m(t)$ where ϵw_m is small in comparison with w_0 and search for a solution of (2) such as $h = h_0 + \epsilon h_1(t) + \epsilon^2 h_2(t) + \cdots$. This yields an infinite sequence of identities:

$$\frac{\beta\gamma_2}{f^2}h_0\partial_x h_0 = w_e \qquad (24)$$

$$\partial_t h_1 - \frac{\beta\gamma_2\lambda}{f^2}[h_0\partial x h_1 - h_1\partial_x h_0] = -\lambda w_m \qquad (25)$$

$$\partial_t h_2 - \frac{\beta\gamma_2\lambda}{f^2}[h_0\partial_x h_2 + h_2\partial_x h_0 + 2h_1\partial_x h_1] = 0, \qquad (26)$$

and so on. Equation (24) yields again the stationary solution (23) whereas (25) determines the main propagative part of the response. For harmonic forcing [w_m proportional to $\exp(i\omega t)$], (25) shows that the response is also harmonic with the same frequency. Moreover, as f increases and h_0 decreases northward (the mean thermocline shoals northward), the two effects add and the amplitude of h_1 increases northward. Equation (26) describes the first-order effects of nonlinearity. For harmonic forcing, it implies that h_2 is proportional to $\exp(2i\omega t)$ because of the term $f^{-2}h_1\partial_x h_1$. Therefore, the solution contains a frequency double that of the forcing frequency. The term in the square brakets shows that the amplitude of h_2 increases, when h_1 increases or h_0 decreases, which takes place northward. The importance of the nonlinearities thus increases northward. If the analysis is continued to an higher order, the entire multiple of the fundamental frequency appear. This simple analysis (valid for small ϵ) suggests therefore that the power spectrum will be modified by the energy transfers from low to high frequency. This is illustrated below.

b. Study with the characteristics method

The solution for a time dependent forcing of the form $w_e(t) = w_0 + w_m(t)$ requires initial and boundary conditions. We assume that the state of the ocean is given at $t = 0$ by (23) and that at $t > 0$ the thermocline depth remains equal to H_0 along the eastern coast. Equation (2) is integrated by the method of characteristics, hence replaced by the system of differential equations,

$$dt = ds \qquad dh = -\lambda w_e ds \qquad dx = c_R ds, \qquad (27)$$

where s represents the abscissa along the characteristics. There are two types of characteristics, those issuing from the interior basin and those issuing from the eastern boundary at a time $t_0 > 0$. The former quickly disappear (in a time approximatively equal to L/c_b where L is the zonal size of the basin), while the latter are given by

$$h = H_0 - \int_{t_0}^{t} \lambda w_e(u)\, du$$

$$x = -\frac{\lambda\beta\gamma_2}{f^2}\left(H_0(t - t_0) - \int_{t_0}^{t}\int_{t_0}^{u} \lambda w_e(v)\, dv\, du\right).$$

$$(28)$$

For harmonic forcing $w_n(t) = \epsilon w_0 \cos\omega t$, (28) becomes

$$h = H_0 - \lambda w_0(t - t_0) - \frac{\lambda \epsilon w_0}{\omega}(\sin\omega t - \sin\omega t_0)$$

$$x = -\frac{\lambda \omega \gamma_2}{f^2}\left[H_0(t - t_0) - \frac{\lambda w_0(t - t_0)^2}{2} \right.$$

$$+ \frac{\lambda \epsilon w_0}{\omega^2}(\cos\omega t - \cos\omega t_0)$$

$$\left. - \frac{\lambda \epsilon w_0}{\omega}(t - t_0) \sin\omega t_0 \right]. \qquad (29)$$

Figure 7 ⬤ shows the time evolution of the thermocline depth anomalies at 40°N computed from (29). The forcing period is 10 yr; the mean value w_0 and the amplitude of the Ekman pumping anomaly 30 m yr^{-1} and 12 m yr^{-1}, respectively. The response pattern becomes more elongated as one moves westward, and the positive peaks are slightly more westward than the negative ones. Spectral peaks appear at integral multiples of the forcing frequency (Fig. 8 ⬤), reflecting in spectral space the assymmetry of the ocean response between thermocline shoaling and thickening. These secondary peaks become more energetic northward as nonlinearities become more important, as suggested in section 4a.

To study the response to a stochastic forcing, we could directly integrate (2) with a random forcing term. However, to save computational time and improve accuracy, we use instead relation (28) with a time sampling of 2 months. The forcing is defined as

$$w_e(t) = w_0\left(1 + \epsilon \sum_i \cos(\omega_i t + \phi_i)\right), \qquad (30)$$

where i is an index ranging from 1 to 2500 and we use $w_0 = 30$ m yr^{-1} and $\epsilon = 0.05$. Note that the net perturbation is not small: indeed the value of ϵ has been adjusted so that the random term has maxima of about 1/3. This leads to a realistic amplitude of the variations of the Ekman pumping. The period $T_i = 2\pi/\omega_i$ is randomly chosen between 2 months and 100 years and the phase ϕ_i between 0 and 2π so that the power spectrum of the forcing is white (Fig. 9 ⬤). As shown by Fig. 10 ⬤ (left), the oceanic response is strongly affected by the nonlinearities at 40°N, and a strong whitening is observed at high frequency, reflecting the multiple peaks of Fig. 8 ⬤; that is, the energy transfer is toward higher frequencies. There are two spectral domains where the power is approximatively constant, one at low frequency and the other at high frequency. However, the spectrum would redden at high frequency if dissipation was included. At 20°N (Fig. 10 ⬤, right), the spectrum remains very close to the one predicted by linear theory, because of the thick thermocline [see (26) and the corresponding discussion], so that the peaks and troughs that result from the in phase or out of phase interferences between free and forced waves are still seen.

To confirm this calculation, a 200-yr integration has been performed by Herbaut et al. (2002). with the Massachussets Institute of Technology primitive equation model (Marshall et al. 1997) limited to an idealized basin of constant depth on a sphere. The forcing was stochastic in time but with a standing pattern in space that coarsely mimicked the North Atlantic Oscillation. We show on Fig. 11 ⬤ (left) a spectrum of the 9°C isotherm depth at 42°N and 20° to the east of the western boundary, where the Rossby wave activity is strong. The analogy with Fig. 10 ⬤ (left) is clear. Between 0.5 and 4 years, the spectrum flattens at 42°N as suggested by the nonlinear theory. At lower frequencies, the decay is faster than ω^{-2} because the GCM shows a pronounced peak at a 20-yr period linked both to the standing pattern of the forcing (Jin 1997) and subpolar gyre dynamics (Herbaut et al. 2002). At southern latitudes, in the subtropical gyre, the spectrum decays uniformly as ω^{-2}, as predicted (Fig. 11 ⬤, right).

These results are in agreement with the study of von Storch et al. (2001) who analyzed the spectral properties of climatic variables obtained with various coupled GCMs. They found two types of spectra in their millenium integrations. Type I spectra (characterized by an high frequency ω^{-2} slope and a low-frequency plateau) are characteristic of the upper ocean and the high latitude part of the deep ocean. Type II spectra [characterized by a plateau at high frequency (from 1 to 10 yr^{-} ^{1}) and an $\omega^{-\beta}$ slope at low frequency where β is a positive constant depending on the location, the variable, etc.] are characteristic for variations in the deep midlatitude and tropical ocean. The transition between Type I spectrum and Type II spectrum seems to occur at a depth of about 500 m in the midlatitudes, in an area where the effects of the surface forcing weakens and the internal dynamics of the ocean becomes important. Our study suggests that nonlinear interactions could explain this spectral flattening.

5. Discussion and conclusions

With their simple nondissipative linear model, FMZ found good agreement between the predicted baroclinic response to a zonally independent stochastic wind stress forcing and that computed from a coupled GCM, but a more questionable one with the observations. In this paper, we have extended their model to the first baroclinic mode of a 2.5-layer ideal-fluid model of the ventilated thermocline and studied the impact of dissipation, spatial variations of the forcing, and nonlinearity.

Using the formulation of Qiu et al. (1997) for the horizontal diffusion, it was shown that the dissipation smoothes the spectrum (there are no longer frequencies where the spectral power vanishes) and slightly steepens the spectral decay at high frequency, while barely affecting the low frequencies. Taking into account the spatial variability of the forcing also smoothes the spectrum and modifies it at low frequency: the power no longer increases quadratically with the distance from the eastern coast, but more moderately. For a forcing with a white spatial spectrum, the increase becomes linear. If the forcing has a dominant spatial scale around k_0 (see Fig. 3 ⊙▬ and its discussion), a case that does not appear to be very realistic, the maximum variance is found near $\omega = c_b k_0$, just as in the case of a single standing forcing pattern (Jin 1997).

Lastly, taking into account some of the effect of nonlinearity, namely the dependence of the Rossby wave speed on the depth of the thermocline, results in energy tranfers from one frequency to another and a whitening of the spectra at high frequency, which should be strongest at high latitudes. This could explain the shape of the spectra found in the GCM simulations (Fig. 11 ⊙▬ and von Storch et al. 2001) for periods ranging from 0.5 to 5 yr, and it is consistent with the spectral flattening seen at Bermuda. However, the comparison with the observations is difficult since our model is only applicable to the low frequencies and sufficiently long time series are very sparse. At high frequency or small spatial scale (less than 500 km), the $|\omega|^{-2}$ spectral decay seems to be controlled by the nonlinear interactions between eddies (e.g., Rhines 1975), which are not represented in our model. Clearly the latter can only explain part of the observed spectral characteristics at low frequencies (from annual to interdecadal). It would need to represent the nonlinear interactions with the barotropic and higher baroclinic modes, as well as topographic effects, to be applicable to a broader frequency range.

REFERENCES

Frankignoul C., and P. Müller, 1979: Quasi-geostrophic response of an infinite β-plane ocean to stochastic forcing by the atmosphere. *J. Phys. Oceanogr.*, **9**, 104–127. Find this article online

Frankignoul C., and E. Zorita, 1997: A simple model of the decadal response of the ocean to stochastic wind stress forcing. *J. Phys. Oceanogr.*, **27**, 1533–1546. Find this article online

Gradshteyn I. S., and I. M. Ryzhik, 1965: *Table of Integral Series and Products*. Academic Press, 1086 pp.

Herbaut C., J. Sirven, and S. Février, 2002: Response of a simplified oceanic general circulation model to idealized NAO-like stochastic forcing. *J. Phys. Oceanogr.,* in press.

Holton J. R., 1992: *An Introduction to Dynamic Meteorology*. 3d ed., International Geophysics Series. Vol. 48, Academic Press, 511 pp.

Jin F. F., 1997: A theory of interdecadal climate variability of the North Pacific ocean–atmosphere system. *J. Climate*, **10**, 1821–1835. Find this article online

Joyce T. M., and P. Robbins, 1996: The long-term hydrographic record at Bermuda. *J. Phys. Oceanogr.*, **26**, 3121–3131. Find this article online

Large W. G., W. R. Holland, and J. C. Evans, 1991: Quasigeostrophic ocean response to real wind forcing: The effects of temporal smoothing. *J. Phys. Oceanogr.*, **21**, 998–1017. Find this article online

Levitus S., 1989: Interpentadal variability of temperature and salinity at intermediate depths of the North Atlantic Ocean, 1970–1974 versus 1955–1959. *J. Geophys. Res.*, **94**, 6091–6131. Find this article online

Marshall J., A. Adcroft, C. Hill, L. Perelmn, and C. Heisey, 1997: A finite volume incompressible Navier–Stokes model for studies of the ocean on parallel computers. *J. Geophys. Res.*, **102**, 5753–5766. Find this article online

Qiu B., W. Miao, and P. Müller, 1997: Propagation and decay of forced and free baroclinic rossby waves in off-equatorial oceans. *J. Phys. Oceanogr.*, **27**, 2405–2417. Find this article online

Rhines P. B., 1975: Waves and turbulence on a β-plane. *J. Fluid Mech.*, **69**, 417–443. Find this article online

Sirven J., and C. Frankignoul, 2000: Variability of the thermocline due to the sudden change in the Ekman pumping. *J. Phys. Oceanogr.*,

30, 1776–1789. Find this article online

Sturges W., and B. G. Hong, 1995: Wind forcing of the Atlantic thermocline along 32°N at low frequencies. *J. Phys. Oceanogr.*, **25**, 1706–1715. Find this article online

von Storch J. S., V. V. Kharin, U. Cubasch, G. C. Hegerl, D. Schriever, H. von Storch, and E. Zorita, 1997: A description of a 1260-year control integration with the coupled ECHAM1/LSG general circulation model. *Climate Dyn.*, **10**, 1525–1543. Find this article online

von Storch J. S., P. Müller, and E. Bauer, 2001: Climate variability in millenium integrations with coupled atmosphere ocean GCMs: A spectral view. *Climate Dyn.*, **10**, 1525–1543. Find this article online

Zorita E., and C. Frankignoul, 1997: Modes of the North Atlantic decadal variability in the ECHAM1/LSG coupled ocean–atmosphere general circulation model. *J. Climate*, **10**, 183–200. Find this article online

---

APPENDIX A

6. Derivation of the Wave Equation

As shown in Sirven and Frankignoul (2000), geostrophy, hydrostatic equilibrium, and the Boussinesq approximation lead to the time-dependent Sverdrup relation

$$\frac{\partial H}{\partial t} - \frac{\beta}{f^2}\left(\gamma_1 h_1 \frac{\partial h_1}{\partial x} + \gamma_2 H \frac{\partial H}{\partial x}\right) = -w_e. \quad (A1)$$

North of the subduction line, h_1 vanishes and (A1) completely determines the flow. South of it, conservation of potential vorticity in the second layer, $\zeta = f/h_2$, must be added:

$$\frac{\partial \zeta}{\partial t} - \frac{\gamma_2}{f}\frac{\partial H}{\partial y}\frac{\partial \zeta}{\partial x} + \frac{\gamma_2}{f}\frac{\partial H}{\partial x}\frac{\partial \zeta}{\partial y} = 0. \quad (A2)$$

Combining (A1) and $\zeta = /h_2$ yields the wave equation for the effective depth $\mathcal{H} = \sqrt{(\gamma_1/\gamma_2)h_1^2 + H^2}$:

$$\frac{\partial \mathcal{H}}{\partial t} - c_1\frac{\partial \mathcal{H}}{\partial x} = -\lambda w_e - \mu, \quad (A3)$$

where $\lambda = (\partial H/\partial \mathcal{H})^{-1}$, $c_1 = \lambda\beta\gamma_2\mathcal{H}/f^2$, and $\mu = \lambda(\partial H/\partial \zeta)\partial \zeta/\partial t$. The effective depth is linked to the averaged velocity $\mathbf{v}_a = (h_1\mathbf{v}_1 + h_2\mathbf{v}_2)/H$ by the relation $H\mathbf{v}_a = (\gamma_2/2f)\mathbf{k} \times \text{grad}_h(\mathcal{H})^2$ ($\mathbf{k}$ indicates a unit vertical vector). Thus it characterizes the overall response of the thermocline to a variation in w_e and defines the first baroclinic mode. As discussed in Sirven and Frankignoul (2000), the influence of the temporal variations of the potential vorticity via the second baroclinic mode, represented by μ in (29), is small and can be neglected.

To simplify further,

$$\lambda = \left(\frac{\partial H}{\partial \mathcal{H}}\right)^{-1} = \frac{\gamma_2 H + \gamma_1 h_1}{\sqrt{\gamma_2^2 H^2 + \gamma_1\gamma_2 h_1^2}} \quad (A4)$$

is assumed to be constant in time (it is equal to 1 north of the subduction line since h_1 is equal to 0 and peaks to 1.3 south of the subduction line). These assumptions lead to the nonlinear nondissipative wave equation (2).

APPENDIX B

7. Response Spectrum for a Forcing Spectrum Decaying as k^{-2}

If the wind stress curl spectrum has the form (21), (14) can be integrated over k. Using the change of variable $(k - k_b)x = u$, one finds

$$S(\omega) = \int_{-\infty}^{+\infty} \frac{S_0 k_M}{\pi \left[k_M^2 + \left(\dfrac{u}{x} + k_b \right)^2 \right] [(uc_b/x)^2 + \omega_d^2]} \left[(1 - e^{x/x_e})^2 + 4e^{x/x_e} \sin^2 \frac{u}{2} \right] \frac{du}{x}. \tag{B1}$$
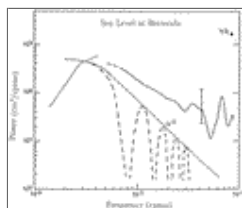
(Click the equation graphic to enlarge/reduce size)

At low frequency, x_e can be considered to be infinite and ω_d and ω tend to zero, yielding:

$$S(\omega) = \frac{S_0 k_M x^3}{\pi c_b^2} \int_{-\infty}^{+\infty} \frac{1}{k_M^2 x^2 + u^2} \frac{\sin^2(u/2)}{(u/2)^2} du. \tag{B2}$$

Integrating (B2) leads to relation (22) (Gradshteyn and Ryzhyk 1965, p. 449).

Figures

Click on thumbnail for full-sized image.

FIG. 1. Frequency spectrum of sea level at Bermuda (after Sturges and Hong 1995). Thick line: the full curve shows a calculation from the continuous portion of data beginning in 1944, smoothed by three Hanning passes (the 99% confidence interval is indicated), except for the last point (dashed); the dotted segment at low frequencies was obtained using gappy data extending back to 1932. The prediction by the linear stochastic model of FMZ for the low frequencies (continuous line) and the high frequency slope in ω^{-2} (dashed line) are also indicated
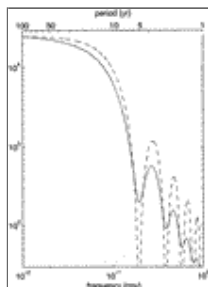
Click on thumbnail for full-sized image.

FIG. 2. Baroclinic pressure spectrum with (continuous curve) and without (dotted curve) dissipation at 3800 km from the eastern coast ($R_b = 34$ km, $\beta = 2 \times 10^{-11}$ m^{-1} s^{-1}, $f_0 = 7 \times 10^{-5}$ s^{-1}, $S_0 = 4.8 \times 10^{-32}$ Pa^2 m^{-4} s^{-2}/cpy)
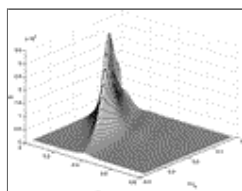
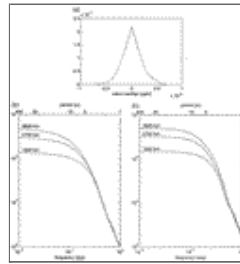Click on thumbnail for full-sized image.

FIG. 3. Frequency–wavenumber spectrum $S(k, x, \omega)$ for $x = -3000$ km and $c_b = 2$ cm s^{-1}. A peak is found for $\omega_0 = c_b k_0$ (and more generally along the line $\omega = c_b k$)
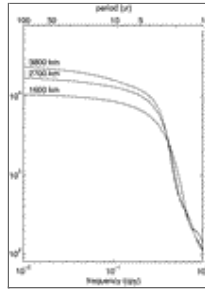
FIG. 4. Baroclinic pressure spectrum with dissipation for a forcing with a white spatial spectrum (R_b = 34 km, $\beta = 2 \times 10^{-11}$ m^{-1} s^{-1}, $f_0 = 7 \times 10^{-5}$ s^{-1}, $S_0 = 4.8 \times 10^{-32}$ Pa^2 m^{-4} s^{-2}/cpy). Note the linear increase of the power at low frequency.

FIG. 5. (a) Spatial spectrum of the wind stress curl in the ECHAM1/LSG simulation (unit: Pa m^{-1}). (b) Corresponding baroclinic pressure spectrum with dissipation. (c) Corresponding baroclinic pressure spectrum without dissipation (R_b = 34 km, $\beta = 2 \times 10^{-11}$ m^{-1} s^{-1}, $f_0 = 7 \times 10^{-5}$ s^{-1}, $S_0 = 4.8 \times 10^{-32}$ Pa^2 m^{-4} s^{-2}/cpy). Note the strong similiraty between the two curves.
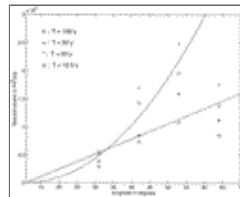
FIG. 6. Spectral power of the baroclinic pressure response in the ECHAM1/LSG at periods 12.5, 20, 50, and 100 yr at various longitudes. The straight line is obtained from a best linear fit and the parabola is deduced form the straight line using $2\pi/k_M =$ 4000 km (see the text for more details).
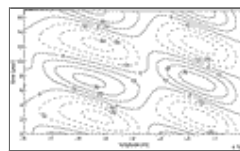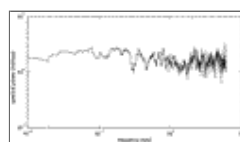
FIG. 7. Time–longitude diagram of the thermocline depth anomalies induced by an harmonic forcing with a 10-yr period (units: m)
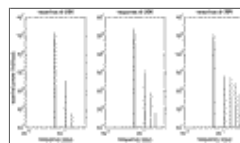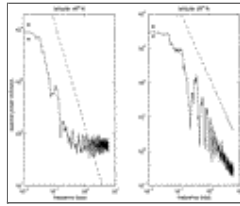
FIG. 8. Spectrum of thermocline depth fluctuations at latitudes 20°N, 30°N, and 40°N

FIG. 9. Forcing spectrum used for the study of the nonlinear response of the ocean to a stochastic forcing

Click on thumbnail for full-sized image.

FIG. 10. Spectrum of thermocline depth fluctuations at 40°N (left) and at 20°N (right). The 99% confidence interval and the frequency slope in ω^{-2} (dashed line) are indicated
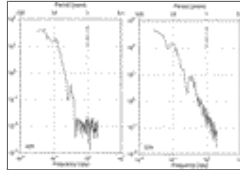
Click on thumbnail for full-sized image.

FIG. 11. Spectra of the 9° isotherm depth fluctuations at 42°N (left) and 11° isotherm depth fluctuations at 37°N (right) computed from a 200-yr integration performed with a simple oceanic GCM

Corresponding author address: Dr. Jérôme Sirven, Laboratoire d' Océanographie Dynamique et de Climatologie, Université Pierre et Marie Curie, T. 15, étage 2, CC100, 4 Place Jussieu, 75252 Paris Cedex 05, France. E-mail: js@lodyc.jussieu.fr

top ▲